ACS Infectious Diseases

pubs.acs.org/journal/aidcbc Article

The Discovery and Development of Thienopyrimidines as Inhibitors of *Helicobacter pylori* That Act through Inhibition of the Respiratory Complex I

Alex K. Mugengana,[▽] Nicole A. Vita,[▽] Autumn Brown Gandt,[▽] Kevin Moran, George Agyapong, Lalit K. Sharma, Elizabeth C. Griffith, Jiuyu Liu, Lei Yang, Ekaterina Gavrish, Kirk E. Hevener, Michael D. LaFleur, and Richard E. Lee*

Cite This: *ACS Infect. Dis.* 2021, 7, 1044−1058 Read Online

ACCESS | Metrics & More | Article Recommendations | Supporting Information

ABSTRACT: The successful treatment of *Helicobacter pylori* infections is becoming increasingly difficult due to the rise of resistance against current broad spectrum triple therapy regimens. In the search for narrow-spectrum agents against *H. pylori*, a high-throughput screen identified two structurally related thienopyrimidine compounds that selectively inhibited *H. pylori* over commensal members of the gut microbiota. To develop the structure−activity relationship (SAR) of the thienopyrimidines against *H. pylori*, this study employed four series of modifications in which systematic substitution to the thienopyrimidine core was explored and ultimately side-chain elements optimized from the two original hits were merged into lead compounds. During the development of this series, the mode of action studies identified *H. pylori*'s respiratory complex I subunit NuoD as the target for lead thienopyrimidines. As this enzyme complex is uniquely essential for ATP synthesis in *H. pylori*, a homology model of the *H. pylori* NuoB−NuoD binding interface was generated to help rationalize the SAR and guide further development of the series. From these studies, lead compounds emerged with increased potency against *H. pylori*, improved safety indices, and a good overall pharmacokinetic profile with the exception of high protein binding and poor solubility. Although lead compounds in the series demonstrated efficacy in an *ex vivo* infection model, the compounds had no efficacy in a mouse model of *H. pylori* infection. Additional optimization of pharmacological properties of the series to increase solubility and free-drug levels at the sequestered sites of *H. pylori* infection would potentially result in a gain of *in vivo* efficacy. The thienopyrimidine series developed in this study demonstrates that NuoB−NuoD of the respiratory complex I can be targeted for development of novel narrow spectrum agents against *H. pylori* and that thienopyrimines can serve as the basis for future advancement of these studies.

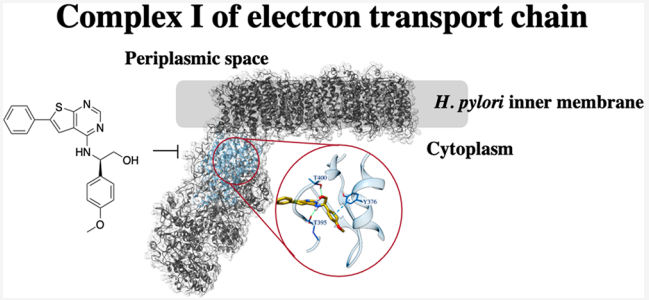

KEYWORDS: *Helicobacter pylori, thienopyridine, NuoD, complex I inhibitor*

Helicobacter pylori is a major causative agent of gastritis, peptic ulcers, and gastric cancer. According to the Centers for Disease Control and Prevention (CDC), more than 500,000 cases of *H. pylori* infections are diagnosed annually in the United States. A triple therapy, consisting of a proton pump inhibitor and the broad-spectrum antibiotics clarithromycin and amoxicillin, is the recommended treatment against *H. pylori* infection.[1] However, the rate of successful treatment with the use of the triple therapy regimen has dropped below 80% due to the rise of antibiotic resistance.[2−5] Additionally, the intensive use of the broad-spectrum antibiotics for the treatment of *H. pylori* infections perturbs the gut microbiome, leading to side effects such as diarrhea and drug resistance in commensal pathogens.[1] Given the rise of *H. pylori* resistance, new drugs are needed for the treatment of *H. pylori* infections.

In a previous effort to discover novel chemical matter selective against *H. pylori*, a high-throughput screening protocol was developed to address the microaerophilic environment required to grow *H. pylori*.[6] Hits found in the high-throughput screening campaign were then screened against *Staphylococcus aureus* to remove promiscuous compounds and prioritize selective compounds. From this approach, we previously reported Hpi1 (Figure 1A), a selective anti-*H. pylori* compound with excellent *in vitro* potency

Special Issue: Gut Pathogens

Received: May 11, 2020
Published: January 20, 2021

https://dx.doi.org/10.1021/acsinfecdis.0c00300
ACS Infect. Dis. 2021, 7, 1044−1058

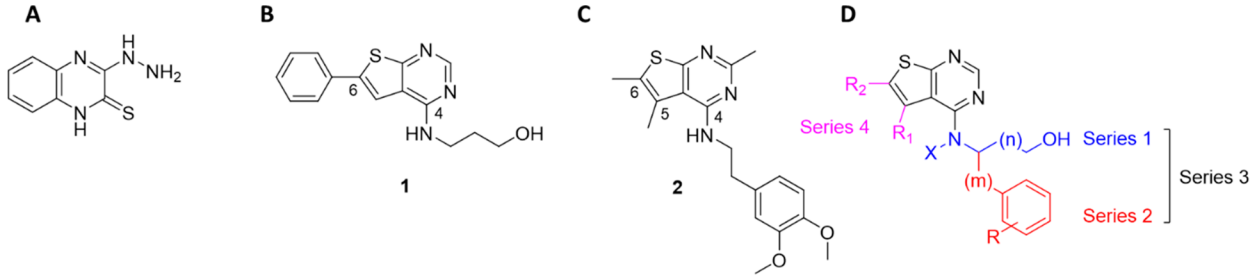

Figure 1. (A) Structure of Hpi1, a selective anti-*H. pylori* compound that emerged as a positive hit from a high-throughput screen against *H. pylori*.[6] (B, C) Structures of thienopyrimidines hits **1** and **2** that were identified using a similar screening approach with the *H. pylori* IC_{50} of 1.55 and 1.72 μM, respectively. (D) Areas substituted in this study to improve potency, drug-like properties, and cytotoxicity.

Scheme 1. Synthesis of Thienopyrimidine Derivatives[a]

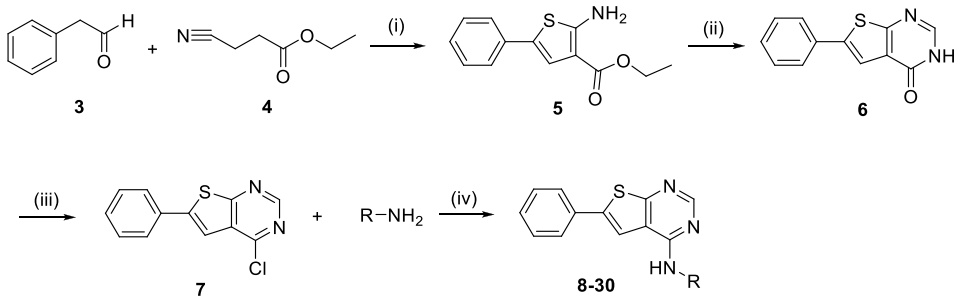

[a]Reagents and conditions: (i) sulfur, morpholine, ethanol, 70 °C, microwave, 20 min, 90%; (ii) formamide, reflux, 18 h, 80%; (iii) $POCl_3$, *N,N*-dimethylaniline, reflux, 14 h, 90%; (iv) ethanol, 150 °C, microwave, 1 h, 80−93%.

(*H. pylori* minimum inhibitory concentration (MIC) of 0.002 μg/mL) compared to clarithromycin (0.008 μg/mL).[6] This protocol was subsequently applied to a larger library of 219,197 compounds, which yielded 2027 compounds as positive hits. The hit compounds were clustered and subsequently prioritized on the basis of their solubility and their chemical tractability. The second screen identified two thienopyrimidine compounds, **1** and **2** (Figure 1B,C), with an *H. pylori* 50% inhibitory concentration (IC_{50}) of 1.55 and 1.72 μM, respectively. Their activities were confirmed through resynthesis and testing.

Herein, we report the structure−activity relationship (SAR) developed from the modification of thienopyrimidines **1** and **2** against *H. pylori*, which explored substitutions around the thienopyrimidine core and merged optimized side-chain elements from the two hits. Hit to lead development was based on *H. pylori* activity, cytotoxicity, and *in vivo* and *ex vivo* efficacy using a mouse model of infection. During these studies, NADH/ubiquinone oxidoreductase (complex I) subunit NuoD was identified as a putative target of the thienopyrimidine series by analyzing resistant mutants using whole-genome sequencing and performing genetic transformation and complementation of resistance. To help rationalize the SAR, explore the mechanism of action, and guide further development of the series, a homology model of the *H. pylori* NuoB−NuoD binding interface was generated. These studies produced tractable thienopyrimidine leads with a defined mechanism of action suitable for further optimization and validated the NuoB−NuoD interface as a target for the development of novel narrow spectrum agents against *H. pylori*.

RESULTS AND DISCUSSION

Generation of Optimized Thienopyrimidines. Four series of new compounds were synthesized to develop the SAR around the two thienopyrimidine hits as outlined in Schemes 1−3.[7−10] Initial SAR efforts focused on examining the *N*-alkyl hydroxyl moiety of hit compound **1**, series-1 (Table 1), and the phenethylamine motif of compound **2**, series-2 (Table 2). Side chains based on lead compounds from each series were then merged into compounds for series-3 (Table 3). Finally, series-4 explored the differing substitution patterns observed for compounds **1** and **2** at C5 and C6 of the thienopyrimidine ring in combination with an optimized phenylglycinol 4-position side chain from series-3 (Table 4).

To generate compounds in series-1−3 (Scheme 1), phenylacetaldehyde **3** was reacted with ethyl 3-cyanopropanoate **4** to give phenylthiophene **5**. Heating **5** in excess formamide formed pyrimidone **6**. Chlorination and dehydration of the pyrimidone with phosphoryl chloride afforded chlorothienopyrimidine **7**, which was coupled with a variety of primary amines and a secondary amine to give targeted 4-position substituted *H. pylori* inhibitors (**8**−**30**). Commercially available amine starting materials with hydroxyl and aromatic moieties, similar to the moieties identified within the hit compounds, were used to synthesize analogs. These amines were selected on the basis of their structural resemblance to the amine substituents of the hit compounds and refined as data from synthesized compounds developed the SAR of each series.

Compounds in each series were evaluated for their activity against *H. pylori* and cytotoxicity (Tables 1−4). Antimicrobial activity was measured using IC_{50} assays against *H. pylori* type strains ATCC 43504 and SS1, a mouse adapted strain used in the mouse model of infection. Activity was also monitored

https://dx.doi.org/10.1021/acsinfecdis.0c00300
ACS Infect. Dis. 2021, 7, 1044−1058

Table 1. Structure-Activity Relationship of Series-1[a]

Compound	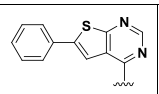	*H. pylori* ATCC 43504 pIC_{50} (M)	*H. pylori* SS1 pIC_{50} (M)	*H. pylori* SS1 NuoD A402P pIC_{50} (M)	FaDu Cells Cytotoxicity pIC_{50} (M)
1	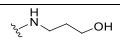	5.8 ± 0.10	5.8 ± 0.037	4.4 ± 0.27	3.9 ± 0.051
8	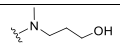	4.8 ± 0.27	5.2 ± 0.15	4.7 ± 0.23	4.0 ± 0.023
9	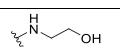	5.3 ± 0.071	5.7 ± 0.081	4.0 ± 0.039	4.0 ± 0.046
10	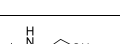	7.4 ± 0.15	7.1 ± 0.24	5.3 ± 0.034	4.0 ± 0.045
11	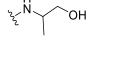	6.0 ± 0.27	6.4 ± 0.16	4.8 ± 0.12	4.2 ± 0.013
12	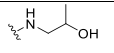	5.3 ± 0.032	5.6 ± 0.12	4.6 ± 0.26	3.6 ± 0.043
13	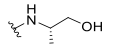	6.8 ± 0.035	7.5 ± 0.10	5.2 ± 0.16	4.5 ± 0.035
14	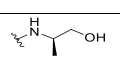	5.9 ± 0.20	6.4 ± 0.16	4.8 ± 0.14	4.5 ± 0.046
15	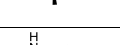	5.8 ± 0.11	6.5 ± 0.10	5.0 ± 0.17	3.9 ± 0.0072
16	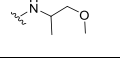	7.0 ± 0.063	7.7 ± 0.17	5.5 ± 0.21	4.4 ± 0.0011
17	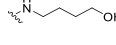	6.1 ± 0.27	6.6 ± 0.15	4.9 ± 0.16	4.4 ± 0.0010
18	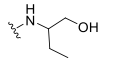	5.5 ± 0.028	6.1 ± 0.048	4.5 ± 0.25	4.3 ± 0.077

[a]All pIC_{50} ($-\log IC_{50}$) data are the mean of at least 3 measurements. Error measured in SEM.

Table 2. Structure-Activity Relationship of Series-2[a]

Compound	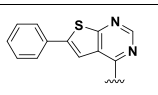	*H. pylori* ATCC 43504 pIC_{50} (M)	*H. pylori* SS1 pIC_{50} (M)	*H. pylori* SS1 NuoD A402P pIC_{50} (M)	FaDu Cells Cytotoxicity pIC_{50} (M)
19	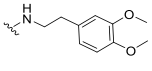	6.8 ± 0.26	7.4 ± 0.035	6.3 ± 0.23	3.9 ± 0.25
20	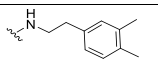	7.1 ± 0.039	6.3 ± 0.20	5.3 ± 0.25	>4.8
21	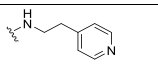	5.6 ± 0.092	5.9 ± 0.17	5.7 ± 0.28	3.9 ± 0.25
22	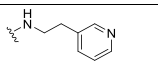	5.2 ± 0.11	5.5 ± 0.088	5.0 ± 0.21	4.0 ± 0.0053
23	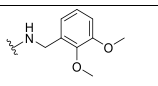	5.8 ± 0.036	6.3 ± 0.17	4.9 ± 0.13	4.6 ± 0.087

[a]All pIC_{50} ($-\log IC_{50}$) data are the mean of at least 3 measurements. Error measured in SEM.

against a target-based resistant mutant *H. pylori* SS1 NuoD A402P to ensure the developing anti-*H. pylori* SAR remained on target. Poor solubility of these 4 compound series sometimes resulted in large standard deviations; therefore, the comparison of the IC_{50} between the two strains served to guide the development of the series, leading to successful identification of lead compounds **25** and **26** with a >69-fold increase in potency for both strains. The IC_{50} data is presented as pIC_{50}, the negative log of the molar IC_{50} value to better follow the emerging SAR.

https://dx.doi.org/10.1021/acsinfecdis.0c00300
ACS Infect. Dis. 2021, 7, 1044−1058

Table 3. Structure-Activity Relationship of Series-3[a]

Compound	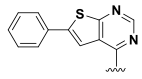	*H. pylori* ATCC 43504 pIC_{50} (M)	*H. pylori* SS1 pIC_{50} (M)	*H. pylori* SS1 NuoD A402P pIC_{50} (M)	FaDu Cells Cytotoxicity pIC_{50} (M)
24	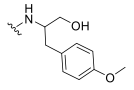	6.9 ± 0.15	6.6 ± 0.057	5.0 ± 0.072	4.8 ± 0.0054
25	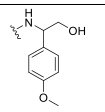	7.7 ± 0.070	7.7 ± 0.044	6.9 ± 0.15	3.4 ± 0.050
26	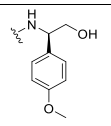	8.0 ± 0.13	8.2 ± 0.093	7.1 ± 0.20	4.8 ± 0.00023
27	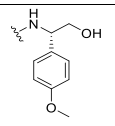	7.3 ± 0.032	7.0 ± 0.13	5.7 ± 0.14	4.3 ± 0.047
28	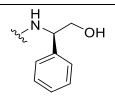	7.6 ± 0.17	8.0 ± 0.23	6.1 ± 0.15	>4.7
29	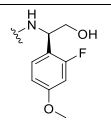	7.7 ± 0.086	7.9 ± 0.040	6.5 ± 0.18	4.5 ± 0.012
30	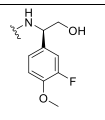	7.8 ± 0.073	7.9 ± 0.055	6.5 ± 0.17	4.5 ± 0.017
31	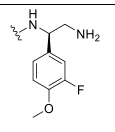	5.5 ± 0.061	6.0 ± 0.20	4.8 ± 0.071	4.3 ± 0.13

[a]All pIC_{50} ($-\log IC_{50}$) data are the mean of at least 3 measurements. Error measured in SEM.

Table 4. Structure-Activity Relationship of Series-4 with Substitution at the 5- and 6-Positions of the Thienopyrimidine Core[a]

Compound	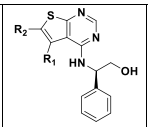		*H. pylori* ATCC 43504 pIC_{50} (M)	*H. pylori* SS1 pIC_{50} (M)	*H. pylori* SS1 NuoD A402P pIC_{50} (M)	Cytotoxicity pIC_{50} (M)
	R_1	R_2				FaDu Cells
37			5.2 ± 0.0084	6.2 ± 0.15	5.1 ± 0.17	>4.7
38			6.5 ± 0.015	7.3 ± 0.056	5.1 ± 0.10	4.7 ± 0.057
39			4.8 ± 0.067	5.1 ± 0.044	4.8 ± 0.20	3.9 ± 0.025
40			5.4 ± 0.044	6.3 ± 0.19	6.0 ± 0.18	4.5 ± 0.13

[a]All pIC_{50} ($-\log IC_{50}$) data are the mean of at least 3 measurements. Error measured in SEM.

https://dx.doi.org/10.1021/acsinfecdis.0c00300
ACS Infect. Dis. 2021, 7, 1044−1058

In series-1, variations to the propyl alcohol motif of compound **1** were evaluated (Table 1). Compound **8** was generated first to investigate the effect of *N*-methylation of the amine group attached at the 4-position of the thienopyrimidine found in hit compound **1**. Compound **8** did not improve the *H. pylori* pIC_{50} values and increased cytotoxicity. Therefore, the free secondary aromatic was retained for the remainder of series-1. To examine the length of the spacer contribution between the hydroxyl group and the amine moiety in **1**, compound **9** was synthesized with a shorter ethyl motif as a spacer and compound **15** was synthesized with a longer spacer that included an additional methylene unit. Neither compound consistently improved the potency compared with **1**.

To investigate the potential for branching between the amine moiety and the hydroxyl group of **1**, methyl branched regio-isomers **10** and **11** were synthesized (Table 1). Compound **10** demonstrated a 20-fold greater potency against *H. pylori* SS1 than **1**, and compound **11** was 4-fold more potent than **1**. The IC_{50} in ATCC 43504 confirmed this with a 37-fold increase in potency for compound **10** and only a negligible less than 2-fold increase for **11**. This suggested there may be a preference for the modification at the amine α-carbon over the β-carbon. The methylation at this amine α-carbon creates a chiral center; therefore, the contribution of each isomer in **10** was determined through the synthesis of enantiomers **12** (*S*) and **13** (*R*). The *R* enantiomer **13** was found to be the active isomer, demonstrating 56-fold increased activity over **1** in SS1, while the *S* enantiomer **12** did not improve the activity over compound **1**. To examine the contribution of the hydroxyl group in **10**, the O-methylated analog **14** was synthesized. Overall, compound **14** demonstrated less potency when compared to **10**. The activity of **14** against ATCC 43504 was 29-fold less potent than **10**. Therefore, the free hydroxyl group was retained in the remainder of this series. The importance of this hydroxyl group was later highlighted in the modeling studies of NuoD in complex with an active ligand (Figure 2).

To determine if a further substitution could be tolerated on the α- and β-carbons of **10** and **11**, regio-isomeric compounds **16** and **17** with an additional methylene unit were generated, respectively. The pIC_{50} values of **16** and **17** were very similar to the parent compounds **10** and **11**, in both SS1 and ATCC 43504, indicating branching can be accommodated at this position. However, compound **18**, with a larger isopropyl substitution over the ethyl motif found in **16**, showed decreased potency. Overall, within compound series-1, clear SAR was observed, consistent with the analogs engaging a defined molecular target. However, increased potency did come with an increase in cytotoxicity for this series. Important to the SAR, and carried forward into the design of series-3 compounds, was a 2-carbon linker between the amine moiety and the hydroxy group, branching at the amine α-carbon over the β-carbon and retaining the terminal hydroxy group.

Series-2 was designed to evaluate the substitution of the phenyl ring in the phenylethyl side chain of compound **2**. Four analogs with varying phenyl substitutions, **19**, **20**, **21**, and **22** (Table 2), were synthesized on the thienopyridine core. Compound **19** displayed improved potency (11-fold against ATCC43504) over compound **2** with a pIC_{50} of 6.8 ± 0.26 (IC_{50} 0.16 μM) and improved cytotoxicity. **19** is the direct phenyl-thienopyrimidine hybrid of **2** with the 3,4-dimethoxyphenethyl side chain. Substitution of the dimethoxyphenyl motif with dimethylphenyl, compound **20**, decreased comparative potency and increased cytotoxicity. Three and four substituted pyridyl analogs **21** and **22** were designed to increase metabolic stability and solubility but also showed substantially decreased potency.

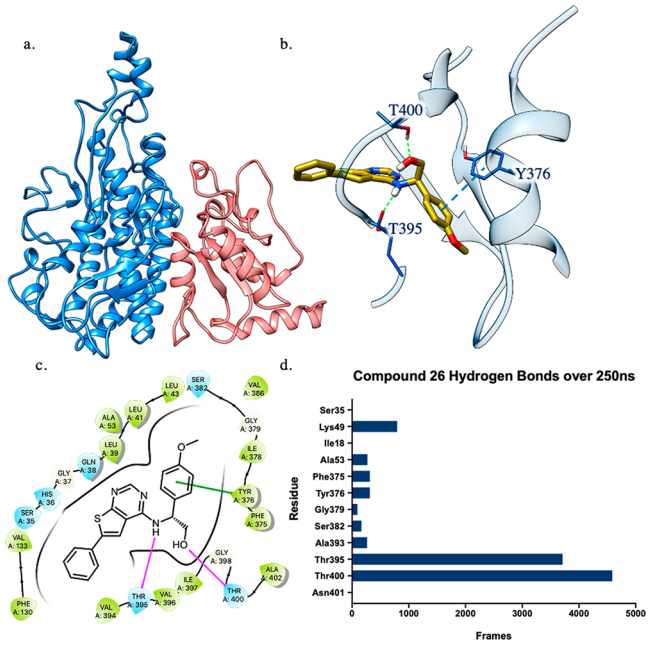

Figure 2. (a) Homology model of the NuoD and NuoB subunits of complex I. (b) Snapshot of lead compound **26** (gold) in the average conformation over a 250 ns molecular dynamic simulation in the wild-type protein. The 250 ns MD simulation shows that compound **26** is a hydrogen bond donor to the carbonyl oxygen at T395 and accepts a hydrogen bond from the hydroxyl side chain of T400 labeled with green dotted lines, respectively. Compound **26** methoxybenzyl group π-stacks with Y376 illustrated with blue dotted lines. (c) A ligand interaction diagram between compound **26** and the protein. Pink lines show hydrogen bonds, and the green lines show $\pi-\pi$ interactions. (d) Analysis of compound **26** hydrogen bond interactions with the respective residues over the entire 250 ns simulation.

The SAR progression revealed series leads **16** and **19** from hits **1** and **2**, respectively. We hypothesized that merging both substituents at the 4-position of phenyl-thienopyrimidine could produce analogs with increased potency. Thus, we synthesized compound **24** (Table 3), which demonstrated activity similar to **16** and **19** against ATCC 43504 but weaker activity against the SS1 strain. Series-3 was designed to evaluate the modifications of hybrid analogs based on **24** (Table 3). First, compound **25** with a shorter spacer between the aryl motif and the amine was generated, which demonstrated high potency with pIC_{50} 7.7 ± 0.070 (IC_{50} 0.021 μM). To evaluate the contribution of each enantiomer, compounds **26** and **27** were synthesized. Although the difference in magnitude is less, like enantiomers **12** and **13**, compound **26** pIC_{50} ATCC43504 8.0 ± 0.13 and SS1 8.2 ± 0.093 (0.010 μM and 0.0068 μM, respectively), retains the activity of **25**, while the *S* enantiomer **27** decreases activity consistently in both strains ATCC43504 7.3 ± 0.032 and SS1 7.0 ± 0.13 (0.053 μM and 0.11 μM respectively). Unexpectedly, the cytotoxicity of **25** was less than each individual isomer (**26** and **27**), which was reproducible upon resynthesis and testing. The reason for this observation is unclear at this time. Unsubstituted **28** retained the reasonable potency of the series-3 compounds with an pIC_{50} 7.6 ± 0.17 (IC_{50} of 0.023 μM). Fluorinated

https://dx.doi.org/10.1021/acsinfecdis.0c00300
ACS Infect. Dis. 2021, 7, 1044−1058

Scheme 2. Synthesis of Amine Derivative 31[a]

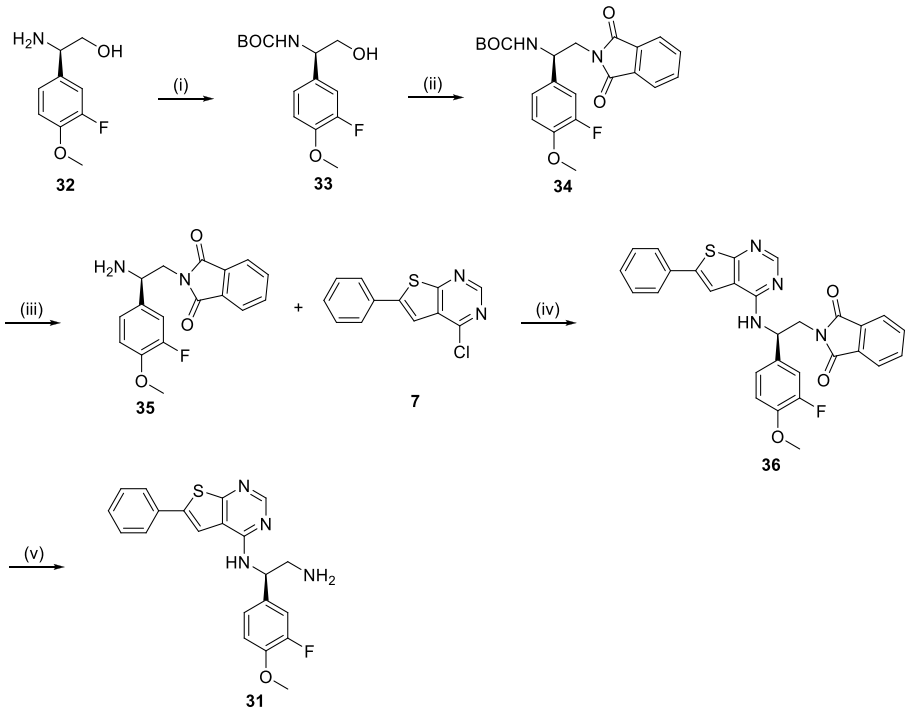

[a]Reagents and conditions: (i) di-*tert*-butyl dicarbonate, Et_3N, DCM, RT, 2 h; (ii) phthalimide, DIAD, Ph_3P, DCM, RT, 4 h; (iii) 4 M HCl in dioxane, DCM, methanol, RT, 4 h; (iv) Et_3N, reflux, 6 h; (v) NH_2NH_2, methanol, RT, 6 h.

Scheme 3. Synthesis of Thienopyrimidine Derivatives with Modifications at Positions 5 and 6[a]

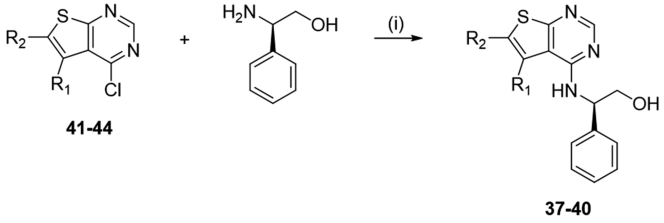

41: R_1= H_3C—, R_2= H_3C—
42: R_1= H_3C—, R_2= 
43: R_1=  , R_2= H_3C—
44: R_1=  , R_2= H—

37: R_1= H_3C—, R_2= H_3C—
38: R_1= H_3C—, R_2= 
39: R_1=  , R_2= H_3C—
40: R_1=  , R_2= H—

[a]Reagents and conditions: (i) Et_3N, 150 °C, microwave, 1 h, 89−93%.

compounds **29** and **30** were synthesized in efforts to increase metabolic stability. Fluorination in these compounds was tolerated as both retained similar IC_{50} values to **26**, which may be useful in the future development of this series.

The final compound synthesized in series-3 was compound **31**, the primary amine analog of **30**. It was generated to explore the potential of amine replacement, as primary amines have been shown to enhance the uptake of drugs into Gram-negative bacteria.[11] Compound **31** was synthesized as described in Scheme 2, starting from amino alcohol intermediate **32**, Boc-protection yielded alcohol **33**.[12,13] Substitution of the hydroxyl group of **33** with a phthalimide group was carried out under Mitsunobu conditions to give the intermediate **34**. Next, the removal of the Boc protecting group yielded the amine **35**, which was coupled to chlorothienopyrimidine **7** to afford the intermediate **36**. In the final step, the deprotection of the phthalimide group of **36** afforded the targeted thienopyrimidine **31**. The substitution of the hydroxyl group for a primary amine resulted in a large increase (>79-fold for both SS1 and ATCC 43504) in the *H. pylori* IC_{50}, indicating that the amine replacement was not tolerated and the hydroxyl group is required to maintain the low nM potency observed in the other compounds in series-3. This concurs with the modeling data for **26** (Figure 2), showing the hydroxyl group acting as a hydrogen bond acceptor to the T400 residue.

Series-3 confirmed our hypothesis that the lead side chains from series-1 and series-2 could be combined, producing leads

https://dx.doi.org/10.1021/acsinfecdis.0c00300
ACS Infect. Dis. 2021, 7, 1044−1058

with low nM anti-*H. pylori* activity. Like compounds **12** and **13** in series-1, the *R* enantiomer was found to be more potent but again led to an increase in cytotoxicity. Substitution of the phenyl ring was tolerated, which suggests a modification of the phenyl ring may be possible for the development of future compounds with improved metabolic stability. Unfortunately, the replacement of the hydroxyl with the primary amine was not tolerated.

Compounds in series-4 explored the differing substitution patterns observed for compounds **1** and **2** at C5 and C6 of the thienopyrimidine ring, in combination with the phenylglycinol 4-position side chain from series-3 compound **28**. Compounds **37**−**40** were synthesized as described in Scheme 3, and their activities were compared to compound **28** with the simplified phenylglycinol substitution (Table 4). Commercially available chlorothienopyrimidines (**41**−**44**) were used in the coupling reaction with the optimized phenylglycinol side chain to yield the final compounds (**37**−**40**). Moving the phenyl ring to the 5-position (**39** and **40**) substantially reduced anti-*H. pylori* potency. The dimethyl analog **37** with a similar substitution pattern of compound **2** was not as active as compound **28**, instead having similar activity to compound **2**. Compound **38** with a similar phenyl substitution pattern to series-3 compounds and an additional methyl substitution, demonstrated somewhat decreased activity compared to **28**. These data suggested the phenyl ring at the 6-position is preferred, and the 5-position can be a hydrogen or methyl but not a larger phenyl group, possibly due to steric clashes in the NuoB−NouD menaquinone binding tunnel targeted by these inhibitors.

Thienopyrimidines Inhibit *H. pylori* Respiratory Complex I. To determine the target of the thienopyrimidines, one resistant *H. pylori* mutant was successfully isolated by serial passaging (five times) on agar medium containing increasing concentrations of compound **1** and two additional spontaneous first-step mutants were obtained by plating on compound **28**. Whole genome sequencing indicated mutations in NuoD with no other mutations present in all three strains compared to the isogenic wild-type. The serial passage mutant had multiple nonsynonymous mutations in *nuoD*, while the two first-step resistant mutants had single nucleotide polymorphisms in *nuoD* causing an amino acid change, either A402P or T400I (Figure 3). Seven additional resistant mutants were generated using compound **28**, all with a nonsynonymous single-nucleotide polymorphism in *nuoD*, which resulted in amino acid mutations T400I or A402P. Further, the A402P mutation generated by compound **28** was transformed into a drug susceptible strain of *H. pylori* for site directed resistance studies to confirm that resistance was caused by nonsynonymous mutations in *nuoD*. IC_{50} studies with this strain demonstrated resistance was transferable with the A402P mutation alone.

To validate that all the compounds in the thienopyrimidine series were on target, each analog was tested against the mutant *H. pylori* strain SS1 NuoD A402P (Tables 1−4, Figure S1). All of the compounds tested demonstrated significantly decreased anti-*H. pylori* activity against the NuoD mutant strain, with the exception of compounds **8**, **21**, **22**, **39**, and **40**, which did not demonstrate statistical significance, indicating that the mechanism of the action is largely consistent throughout the compound series (Supplementary data, Figure S1). The gene *nuoD* encodes for the NuoD subunit of NADH/quinone oxidoreductase, also known as respiratory complex I.[14−17] These results suggest that complex I, the protein that catalyzes the first step of oxidative phosphorylation, is the putative target of thienopyrimidines.[18,19] Interestingly, NuoD is also the putative target of a previously described series of benzimidazole anti-*H. pylori* agents, with resistance conferring mutations found at NuoD: G398S, F404S, and V407M (Figure S2).[20,21] This group further determined that, while *nuoD* is essential in *H. pylori*, it is dispensable in other bacteria, suggesting that targeting NuoD may spare the microbiome. In accordance with this, we found that compounds **25**, **26**, **28**, **29**, **30**, and **31** had limited to no activity (MIC ≥ 16 μg/mL) against a panel of representative Gram-negative and Gram-positive species, including commensals (Supplementary data, Table S3).

Figure 3. Sequence alignment of the wild-type *nuoD* and two *H. pylori* mutants. Resistant mutants were generated by exposing *H. pylori* to compound **1** or **28** on agar plates. Whole genome sequencing was performed, and single nucleotide polymorphism analysis identified two spontaneous mutants, which had nonsynonymous point mutations in *nuoD*. The resulting amino acid changes were threonine to isoleucine (T400I) and alanine to proline (A402P). *nuoD* encodes for the subunit D of NADH/quinone reductase also known as complex I, a membrane protein that catalyzes the first step of oxidative phosphorylation. Complex I is the putative target of the thienopyrimidine series.

Recent advances in the structural characterization of complex I, one of the largest membrane protein complexes known, have now enabled the computational analysis of complex I inhibitors.[22] The complete structure of NADH/ubiquinone oxidoreductase (complex I) from *Thermus thermophilus* was determined by Baradaran et al.; they modeled it in decylubiquinone, showing the key interactions with Y87 and H38, which correspond to Y85 and H36 in *H. pylori*, respectively.[18] A protein sequence alignment showed that the NuoB and NuoD subunits of *H. pylori*'s complex I have a high degree of sequence similarity with *T. thermophilus*' complex I subunits Nqo6 (63% identity) and Nqo4 (43% identity) (Figure S2). As discussed above, we have shown that thienopyrimidine resistance-conferring mutations occur at T400 and A402, positions which fall within the menaquinone-binding pocket (Figures 3 and S3).[23−25] The location of T400I and A402P mutations indicate that the thienopyrimidine series bind in the menaquinone active site. In comparing the published benzimidazole resistance mutations and the two mutations found above, we hypothesize that the menaquinone active site is a target for *H. pylori* therapy.[20]

In order to further characterize interactions of the thienopyrimidine series of inhibitors with *H. pylori*'s complex I, a model of the wild-type protein (subunits NuoD and NuoB) was built using *T. thermophilus*' complex I as a template. Inhibitor binding interactions were modeled by computationally docking **26** into the predicted active site, which showed hydrogen binding to T400. In order to determine stability of the docked pose of **26**, a 250 ns

https://dx.doi.org/10.1021/acsinfecdis.0c00300
ACS Infect. Dis. 2021, 7, 1044−1058

molecular dynamic simulation was run using AMBERMD. Simulation trajectory analysis revealed key ligand−receptor hydrogen bonding interactions with T400 and T395 with π-stacking interactions to Y376, all located within the menaquinone binding pocket (Figure 2b). Additional analysis revealed that the protein−ligand interaction stabilizes at 50 ns and has a stable energy profile (Figure S4), concluding that the menaquinone pocket is the active site of **26**.

To determine the extent of potential selectivity, **26** was also docked into a model of the A402P mutated NuoD subunit using the same methods as the wild-type. A weaker docking score of −4.4, as opposed to −11.5 in the wild-type, was observed, suggesting a significantly reduced affinity of **26** for the mutated subunit.

Pharmacological Properties of anti-*H. pylori* Thienopyrimidines. To examine if the lead thienopyrimidine **26** was suitable for the advancement into animal testing, the pharmacological properties of its racemate **25** were determined for reasons of cost. The *in vitro* ADME and *in vivo* pharmacokinetic properties of **25** were determined.[26−28] The full results of these studies are provided in Tables S1 and S2, respectively. Compound **25** showed good microsomal stability ($t_{1/2}$ = 3.8 h) and permeability (Ave Pe = 239.5 × 10^{-6} cm/s) but has low solubility (1 μM) and was highly bound to human plasma protein (HPPB % = 99). **25** showed good *in vivo* exposure (AUC = 31 907.71 h·ng/mL, Table S2) at a 50 mg/kg intraperitoneal (IP) dose with a lower exposure found upon oral (PO) dosing in mice. The total drug concentration of **25** in the plasma was above its IC_{50} value for more than 8 h by IP dosing. With good plasma exposure, which we believe is required to treat deep seated ulcerative *H. pylori* infections, we proceeded to test **25** in the *H. pylori* murine infection model.[29,30] Further details of this study are provided in Figure S5.[31] Compared to the metronidazole control, **25** did not show efficacy at 50 mg/kg (PO), 50 mg/kg (IP), or 25 mg/kg (IP).[31]

An *ex vivo H. pylori* infection model was used to investigate the lack of efficacy of compound **25** in the *in vivo* infection model. Mice were infected with an *H. pylori* SS1 strain, as described previously; however, instead, the infected stomach tissues were dissected and placed in sterile growth media containing the active compound.[29,30] These experiments were designed to test the effectiveness of compound **25** independent of drug metabolism and excretion. Compound **25** was found to be highly effective in the *ex vivo* model with colony counts below the limit of detection for 6 of the 10 samples (Figure 4). These data suggest that insufficient levels of compound **25** are present at the site of infection in the *in vivo* model and that optimization of the pharmacokinetic properties of the thienopyrimidines series is likely required to demonstrate *in vivo* efficacy.

In summary, we report the synthesis and evaluation of four series of thienopyridines, through which we establish: a clear anti-*H. pylori* SAR at the 4-, 5-, and 6-position of the thienopyrimidine core; identification of potent compounds, including lead compound **26** with an IC_{50} of 0.0068 μM; mode of action studies identifying *H. pylori*'s respiratory complex I as the target of the thienopyrimidines; computational analysis utilizing a NuoD homology model that supported the SAR observed in microbiological studies; the efficacy in an *ex vivo H. pylori* model. The SAR of the thienopyridines occurred iteratively, prior to the development of the NuoD homology model. From these data, it was found that modified side chains

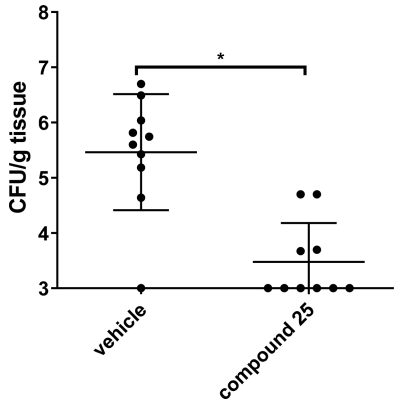

Figure 4. Effect of compound **25** against *H. pylori* in an *ex vivo* infection model. Ten mice were infected with *H. pylori* strain SS1. After 3 days, stomachs were harvested and bisected laterally. One-half of each stomach was placed in a 12-well plate containing either Brucella-FBS medium or Brucella-FBS medium with 0.6 μg/mL (1.6 μM) of compound **25**. Plates were incubated for 24 h, and tissues were washed, homogenized, diluted, and plated for colony counts.

from compounds **1** and **2** on the C4-position of the thienopyrimidine core could be combined to generate more potent compounds. Branching at the amine α-carbon was found to be preferred over the β-carbon with the R enantiomer having greater potency at this position (**13** and **26**). Retention of the hydroxyl group on the amine moiety from compound **1** was required to maintain potency (**14** and **31**), which was shown in modeling studies to form key hydrogen bonding with resistance residue T400 in the NuoD binding site. Fluorination of the phenyl ring in series-3 was tolerated (**29** and **30**), which may be helpful in future development to increase the metabolic stability of these compounds. Finally, the substitution of the C5- and C6-position of the thienopyrimidine ring suggested the phenyl ring at C6 is preferred. This was supported in modeling studies indicating the accommodation for larger groups at C6 but steric hindrance in the binding site for a large substitution at C5.

Utilizing compound **28**, resistance generation, whole-genome sequencing, and resistance transfer studies identified NADH/ubiquinone oxidoreductase (complex I) subunit NuoD as the putative target of the thienopyrimidine series. Complex I, the first protein of the electron transport chain, is located on the inner membrane of *H. pylori* and catalyzes the first step of oxidative phosphorylation. Although complex I is conserved through prokaryotes and eukaryotes, it is uniquely important in *H. pylori* as the electron transport chain is the only pathway to form ATP. Previous research efforts have indicated complex I and NuoD may be a good target for the development of anti-*H. pylori* agents. Researchers at AstraZeneca identified an anti-*H. pylori* benzimidazole series derived from omeprazole (Supplementary data, Figure S6) that targets complex I of the electron transport chain at the same site as the theinopyrimidines.[20,34] In these studies, knockout mutagenesis studies demonstrated that *nuoD* is an essential gene for *H. pylori* but not for the majority of other bacteria, indicating that *H. pylori* can be targeted selectively without perturbation of the host microbiota. Targeting oxidative phosphorylation has been done safely in the clinic, as exemplified by metformin, a drug used for the treatment of diabetes[32] and in the treatment of certain cancers including relapsed/refractory acute myeloid leukemia and solid tumors.[33]

https://dx.doi.org/10.1021/acsinfecdis.0c00300
ACS Infect. Dis. 2021, 7, 1044−1058

These examples, taken together with the studies described herein, suggest that complex I is a worthwhile target in eradicating *H. pylori*, which can now be exploited using structure-based drug design. In this study, the computational model supported the SAR of the thienopyridines developed from the biological studies and can be used going forward in the further development of these agents. Although *in vivo* efficacy could not be obtained for the compounds reported here, **26** is a promising chemical probe that is worth further pharmacological optimization to decrease cytotoxicity and improve *in vivo* efficacy in the *H. pylori* infected mouse model. Toward these goals, ongoing efforts are focused around substituting the thienopyrimidine core with more hydrophilic ring systems.

METHODS

General Chemistry Methods. Starting materials were purchased from Sigma-Aldrich and Enamine. Chemical reactions were monitored by the thin-layer chromatography (TLC) and the Waters ACQUITY-UPLC-MS-UV system. Microwave-assisted chemical reactions were carried out in the Biotage Initiator$^+$. The reaction mixtures were purified using the Biotage Flash column chromatography system with silica cartridges acquired from Biotage Inc. The solvents for chromatography were purchased from Sigma-Aldrich. NMR spectra were obtained using the Bruker 400 MHz NMR spectrometer and the Bruker AVANCE 500 MHz NMR spectrometer. NMR analysis was carried out using the MestReNova software. The chemical shifts and the coupling constants (J) are reported in ppm and hertz (Hz), respectively. The purity of the compounds was determined to be >95% by the UPLC-MS-UV system and NMR. The optical rotation of the chiral compounds was determined using a JASCO P-1010 Polarimeter.

*Ethyl 2-Amino-5-phenylthiophene-3-carboxylate (**5**).* In a microwave tube, ethyl 3-cyanopropanoate **4** (1.771 mL, 16.65 mmol) was added to a solution of 2-phenylacetaldehyde **3** (2 g, 16.65 mmol), sulfur (0.587 g, 18.315 mmol), and morpholine (1.579 mL, 18.315 mmol) in ethanol (20 mL). The resulting mixture was submitted to microwave heating for 30 min at 70 °C. After cooling, the mixture was filtered, and the filtrate was poured in water. The precipitate was collected, dried, and purified by flash column chromatography (Isolera 1, Biotage, 25 g size, elution gradient of 12−60% ethyl acetate in hexanes) to afford **5** as a yellow solid. ^{1}H NMR (DMSO, 500 MHz): δ 7.48−7.44 (m, 4H), 7.33 (t, J = 7.7 Hz, 2H), 7.23 (s, 1H), 7.19 (t, J = 7.4 Hz, 1H), 4.21 (q, J = 7.1 Hz, 2H), 1.28 (t, J = 7.1 Hz, 3H); MS (ESI): m/z 248.5 (M^+ + H).

*6-Phenylthieno[2,3-d]pyrimidin-4(3H)-one (**6**).* Compound **5** (1.15 g, 4.65 mmol) was dissolved in an excess of formamide, and the resulting mixture was heated for 16 h at 160 °C. The mixture was concentrated *in vacuo* and purified by flash column chromatography (Isolera 1, Biotage, 25 g size, elution gradient of 12−60% ethyl acetate in hexanes) to afford **6** as a red solid. ^{1}H NMR ($CDCl_3$, 500 MHz): δ 11.05 (s, 1H), 8.58 (s, 1H), 7.65−7.60 (m, 2H), 7.45 (s, 1H), 7.43−7.38 (m, 2H), 7.33−7.30 (m, 1H); MS (ESI): m/z 230.1 (M^+ + H).

*4-Chloro-6-phenylthieno[2,3-d]pyrimidine (**7**).* Compound **6** (1 g, 4.38 mmol) and *N*,*N*-dimethylaniline (0.043 mL, 0.336 mmol) were dissolved in phosphoryl trichloride (5.10 mL, 54.8 mmol), and the mixture was heated for 16 h to 95 °C. The mixture was concentrated *in vacuo* and purified by flash column chromatography (Isolera 1, Biotage, 25 g size, elution gradient of 12−60% ethyl acetate in hexanes) to afford **7** as a yellow solid. ^{1}H NMR ($CDCl_3$, 500 MHz): δ 8.85 (s, 1H), 7.79−7.77 (m, 2H), 7.62 (s, 1H), 7.54−7.46 (m, 3H); MS (ESI): m/z 247.1 (M^+ + H).

General Procedure for the Amination of 4-Chloro-6-phenylthieno[2,3-*d*]pyrimidine. In a microwave tube, compound **7** (1 equiv), amine (1.5 equiv), and triethylamine (3 equiv) were dissolved in ethanol and subjected to microwave heating for 1 h at 150 °C. The mixture was extracted with ethyl acetate/water, and the organic phase was washed with brine, dried (Na_2SO_4), and concentrated *in vacuo*. The residue was purified by column chromatography (Isolera 1, Biotage, elution gradient of 20−85% ethyl acetate in hexanes) to afford the targeted compound.

*3-((6-Phenylthieno[2,3-d]pyrimidin-4-yl)amino)propan-1-ol (**1**).* Following the general procedure for the amination of 4-chloro-6-phenylthieno[2,3-*d*]pyrimidine, compound **1** was obtained as a white solid. ^{1}H NMR ($CDCl_3$, 400 MHz): δ 8.48 (s, 1H), 7.69−7.67 (m, 1H), 7.67−7.66 (m, 1H), 7.48−7.43 (m, 2H), 7.41−7.37 (m, 1H), 7.33 (s, 1H), 5.70 (br, 1H), 3.85 (q, J = 6.5 Hz, 2H), 3.74 (t, J = 5.9 Hz, 2H), 1.93−1.87 (m, 2H); MS (ESI): m/z 286.1 (M^+ + H).

*3-(Methyl(6-phenylthieno[2,3-d]pyrimidin-4-yl)amino)-propan-1-ol (**8**).* Following the general procedure for the amination of 4-chloro-6-phenylthieno[2,3-*d*]pyrimidine, compound **8** was obtained as a white solid. ^{1}H NMR ($CDCl_3$, 400 MHz): δ 8.41 (s, 1H), 7.74 (s, 1H), 7.70−7.64 (m, 2H), 7.49−7.43 (m, 2H), 7.41−7.36 (m, 1H), 4.67 (br, 1H), 3.96 (dd, J = 6.8, 5.4 Hz, 2H), 3.61−3.60 (m, 2H), 3.51 (s, 3H), 1.96−1.90 (m, 2H); MS (ESI): m/z 301.1 (M^+ + H).

*2-((6-Phenylthieno[2,3-d]pyrimidin-4-yl)amino)ethan-1-ol (**9**).* Following the general procedure for the amination of 4-chloro-6-phenylthieno[2,3-*d*]pyrimidine, compound **9** was obtained as a white solid. ^{1}H NMR ($CDCl_3$, 400 MHz): δ 8.45 (d, J = 2.7 Hz, 1H), 7.72−7.60 (m, 2H), 7.43 (ddt, J = 9.5, 7.8, 1.5 Hz, 2H), 7.40−7.30 (m, 2H), 5.70 (s, 1H), 3.93 (dt, J = 5.0, 3.3 Hz, 2H), 3.82 (ddt, J = 7.2, 5.4, 3.0 Hz, 2H); MS (ESI): m/z 273.1 (M^+ + H).

*2-((6-Phenylthieno[2,3-d]pyrimidin-4-yl)amino)propan-1-ol (**10**).* Following the general procedure for the amination of 4-chloro-6-phenylthieno[2,3-*d*]pyrimidine, compound **10** was obtained as a white solid.^{1}H NMR ($CDCl_3$, 400 MHz): δ 8.38 (s, 1H), 7.62−7.57 (m, 2H 1.32 (d, J = 6.8 Hz, 3H), 7.37 (ddd, J = 7.7, 6.6, 1.6 Hz, 2H), 7.31−7.25 (m, 2H), 5.24 (d, J = 6.7 Hz, 1H), 4.42−4.40 (m, 1H), 3.81 (dd, J = 10.9, 3.1 Hz, 1H),3.68−3.64 (m, 1H); MS (ESI): m/z 286.9 (M^+ + H).

*1-((6-Phenylthieno[2,3-d]pyrimidin-4-yl)amino)propan-2-ol (**11**).* Following the general procedure for the amination of 4-chloro-6-phenylthieno[2,3-*d*]pyrimidine, compound **11** was obtained as a white solid. ^{1}H NMR (DMSO, 400 MHz): δ 8.33 (s, 1H), 8.12 (s, 1H), 7.99 (t, J = 5.9 Hz, 1H), 7.69 (d, J = 7.5 Hz, 2H), 7.51 (t, J = 6.8 Hz, 2H), 7.42−7.38 (m, J = 7.5 Hz, 1H), 4.86 (d, J = 4.8 Hz, 1H), 3.94−3.89 (m, 1H), 3.54−3.38 (m, 2H), 1.13 (d, J = 6.2 Hz, 3H); MS (ESI): m/z 268.7 (M^+ + H).

*(S)-2-((6-Phenylthieno[2,3-d]pyrimidin-4-yl)amino)-propan-1-ol (**12**).* Following the general procedure for the amination of 4-chloro-6-phenylthieno[2,3-*d*]pyrimidine, compound **12** was obtained as a white solid. ^{1}H NMR ($CDCl_3$, 400 MHz): δ 8.47 (s, 1H), 7.71−7.68 (m, 2H), 7.46 (t, J = 7.5 Hz, 2H), 7.41−7.39 (m, 1H), 7.35 (s, 1H), 5.31 (s, 1H), 4.51−4.49 (m, 1H), 3.91 (dd, J = 11.1, 3.02 Hz, 1H), 3.75 (dd, J =

https://dx.doi.org/10.1021/acsinfecdis.0c00300
ACS Infect. Dis. 2021, 7, 1044−1058

11.1, 6.2 Hz, 1H), 1.41 (d, J = 6.9 Hz, 3H); MS (ESI): m/z 286.9 (M^+ + H).

*(R)-2-((6-Phenylthieno[2,3-d]pyrimidin-4-yl)amino)-propan-1-ol (**13**).* Following the general procedure for the amination of 4-chloro-6-phenylthieno[2,3-*d*]pyrimidine, compound **13** was obtained as a white solid. ^{1}H NMR ($CDCl_3$, 400 MHz): δ 8.47 (s, 1H), 7.70−7.68 (m, 2H), 7.46 (t, J = 8.2 Hz, 2H), 7.41−7.35 (m, 2H), 5.33 (s, 1H), 4.52−4.48 (m, 1H), 3.93−3.88 (m, 1H), 3.78−3.73 (m, 1H), 1.41 (d, J = 6.4 Hz, 3H); MS (ESI): m/z 286.9 (M^+ + H).

*N-(1-Methoxypropan-2-yl)-6-phenylthieno[2,3-d]-pyrimidin-4-amine (**14**).* Following the general procedure for the amination of 4-chloro-6-phenylthieno[2,3-*d*]pyrimidine, compound **14** was obtained as a white solid. ^{1}H NMR (DMSO, 400 MHz): δ 8.34 (s, 1H), 8.12 (s, 1H), 7.74−7.68 (m, 3H), 7.51 (t, 2H, J = 7.4 Hz), 7.43−7.38 (m, 1H), 4.60−4.53 (m, 1H), 3.52−3.48 (m, 1H), 3.40−3.37 (m, 1H), 3.30 (s, 3H), 1.24 (d, J = 6.7 Hz, 3H); MS (ESI): m/z 300.8 (M^+ + H).

*4-((6-Phenylthieno[2,3-d]pyrimidin-4-yl)amino)butan-1-ol (**15**).* Following the general procedure for the amination of 4-chloro-6-phenylthieno[2,3-*d*]pyrimidine, compound **15** was obtained as a white solid. ^{1}H NMR ($CDCl_3$, 400 MHz): δ 8.47 (s, 1H), 7.67−7.64 (m, 2H), 7.45−7.25 (m, 4H), 5.67 (s, 1H), 3.79 (s, 2H), 3.69 (s, 2H), 2.16 (s, 1H), 1.87−1.84 (m, 2H), 1.75−1.73 (m, 2H); MS (ESI): m/z 301.3 (M^+ + H).

*2-((6-Phenylthieno[2,3-d]pyrimidin-4-yl)amino)butan-1-ol (**16**).* Following the general procedure for the amination of 4-chloro-6-phenylthieno[2,3-*d*]pyrimidine, compound **16** was obtained as a white solid. ^{1}H NMR ($CDCl_3$, 400 MHz): δ 8.45 (s, 1H), 7.70−7.67 (m, 2H), 7.48−7.43 (m, 2H), 7.39 (t, J = 7.48 Hz, 1H), 7.35 (s, 1H), 5.34 (d, J = 7.5 Hz, 1H), 4.33−4.26 (m, 1H), 3.93 (dd, J = 11.1, 3 Hz, 1H), 3.80 (dd, J = 11.1, 5.8 Hz, 1H), 1.88−1.70 (m, 2H), 1.09 (t, J = 7.2 Hz, 3H); MS (ESI): m/z 300.9 (M^+ + H).

*1-((6-Phenylthieno[2,3-d]pyrimidin-4-yl)amino)butan-2-ol (**17**).* Following the general procedure for the amination of 4-chloro-6-phenylthieno[2,3-*d*]pyrimidine, compound **17** was obtained as a white solid. ^{1}H NMR (DMSO, 400 MHz): δ 8.33 (s, 1H), 8.12 (s, 1H), 7.96 (t, J = 5.73 Hz, 1H), 7.70−7.67 (m, 2H), 7.51 (dd, J = 8.41, 7.01 Hz, 2H), 7.42−7.38 (m, 1H), 4.83 (d, J = 5.24 Hz, 1H), 3.70−3.62 (m, 1H), 3.61−3.55 (m, 1H), 3.44−3.37 (m, 1H), 1.58−1.48 (m, 1H), 1.42−1.31 (m, 1H), 0.93 (t, J = 7.4 Hz, 3H); MS (ESI): m/z 300.9 (M^+ + H).

*3-Methyl-2-((6-phenylthieno[2,3-d]pyrimidin-4-yl)amino)-butan-1-ol (**18**).* Following the general procedure for the amination of 4-chloro-6-phenylthieno[2,3-*d*]pyrimidine, compound **18** was obtained as a white solid. ^{1}H NMR ($CDCl_3$, 400 MHz): δ 8.35 (s, 1H), 7.62−7.59 (m, 2H), 7.37 (t, J = 7.2 Hz, 2H), 7.32−7.25 (m, 2H), 5.30 (d, J = 7.7 Hz, 1H), 4.11−4.05 (m, 1H), 3.87−3.75 (m, 2H), 3.48 (m, 1H), 2.10−2.01 (m, 1H), 1.20−0.98 (m, 6H); MS (ESI): m/z 315.01 (M^+ + H).

*N-(3,4-Dimethoxyphenethyl)-6-phenylthieno[2,3-d]-pyrimidin-4-amine (**19**).* Following the general procedure for the amination of 4-chloro-6-phenylthieno[2,3-*d*]pyrimidine, compound **19** was obtained as a white solid. ^{1}H NMR ($CDCl_3$, 400 MHz): δ 8.54 (s, 1H), 7.65 (d, J = 7 Hz, 2H), 7.45 (t, J = 7.04 Hz, 2H), 7.40−7.36 (m, 1H), 7.20 (s, 1H), 6.88−6.78 (m, 3H), 5.28 (br, 1H), 3.95−3.90 (m, 5H), 3.87 (s, 3H), 2.99 (t, J = 7.04 Hz, 2H); MS (ESI): m/z 392.01 (M^+ + H).

*N-(3,4-Dimethylphenethyl)-6-phenylthieno[2,3-d]-pyrimidin-4-amine (**20**).* Following the general procedure for the amination of 4-chloro-6-phenylthieno[2,3-*d*]pyrimidine, compound **20** was obtained as a white solid. ^{1}H NMR (DMSO, 400 MHz): δ 8.37 (s, 1H), 8.07 (t, J = 5.62 Hz, 1H), 8.00 (s, 1H), 7.67 (d, J = 7.52 Hz, 2H), 7.51 (t, J = 8.08 Hz, 2H), 7.40 (t, J = 7.12 Hz, 1H), 7.06−7.05 (m, 2H), 6.99−6.97 (m, 1H), 3.73−3.68 (m, 2H), 2.87 (t, J = 7.49 Hz, 2H), 2.19 (s, 3H), 2.17 (s, 3H); MS (ESI): m/z 361.21 (M^+ + H).

*6-Phenyl-N-(2-(pyridin-4-yl)ethyl)thieno[2,3-d]pyrimidin-4-amine (**21**).* Following the general procedure for the amination of 4-chloro-6-phenylthieno[2,3-*d*]pyrimidine, compound **21** was obtained as a white solid. ^{1}H NMR ($CDCl_3$, 400 MHz): δ 8.56−8.47 (m, 3H), 7.65−7.63 (m, 2H), 7.44−7.41 (m, 2H), 7.38−7.36 (m, 1H), 7.21−7.18 (m, 3H), 5.26 (s, 1H), 3.98−3.93 (m, 2H), 3.05 (t, 2H, J = 7.52 Hz); MS (ESI): m/z 333.1 (M^+ + H).

*6-Phenyl-N-(2-(pyridin-3-yl)ethyl)thieno[2,3-d]pyrimidin-4-amine (**22**).* Following the general procedure for the amination of 4-chloro-6-phenylthieno[2,3-*d*]pyrimidine, compound **22** was obtained as a white solid. ^{1}H NMR ($CDCl_3$, 400 MHz): δ 8.56−8.53 (m, 3H), 7.68−7.65 (m, J = 6.88 Hz, 2H), 7.61 (d, J = 7.91 Hz, 1H), 7.45 (dd, J = 8.45, 6.60 Hz, 2H), 7.40−7.37 (m, 1H), 7.24 (s, 1H), 5.26 (s, 1H) 3.96 (q, J = 6.73, 2H), 3.08 (t, J = 6.96 Hz, 2H); MS (ESI): m/z 333.1 (M^+ + H).

*N-(2,3-Dimethoxybenzyl)-6-phenylthieno[2,3-d]-pyrimidin-4-amine (**23**).* Following the general procedure for the amination of 4-chloro-6-phenylthieno[2,3-*d*]pyrimidine, compound **23** was obtained as a white solid. ^{1}H NMR ($CDCl_3$, 400 MHz) δ 8.54 (s, 1H), 7.69−7.63 (m, 2H), 7.49−7.41 (m, 2H), 7.40−7.33 (m, 1H), 7.30 (d, J = 1.2 Hz, 1H), 7.11−7.00 (m, 2H), 6.94 (dd, J = 7.8, 1.8 Hz, 1H), 5.73 (s, 1H), 4.89 (d, J = 5.6 Hz, 2H), 3.97 (d, J = 0.9 Hz, 3H), 3.92 (d, J = 1.1 Hz, 3H); MS (ESI): m/z 378.02 (M^+ + H).

*3-(4-Methoxyphenyl)-2-((6-phenylthieno[2,3-d]pyrimidin-4-yl)amino)propan-1-ol (**24**).* Following the general procedure for the amination of 4-chloro-6-phenylthieno[2,3-*d*]-pyrimidine, compound **24** was obtained as a white solid. ^{1}H NMR ($CDCl_3$, 500 MHz): δ 8.38 (s, 1H), 7.55 (d, J = 7.65 Hz, 2H), 7.36 (t, J = 7.54 Hz, 2H), 7.30 (t, J = 7.7 Hz, 1H), 7.14−7.11 (m, 3H), 6.80 (d, J = 8.2 Hz, 2H), 5.39 (d, J = 6.25 Hz, 1H), 4.45−4.39 (m, 1H), 3.82 (d, J = 10.8 Hz, 1H), 3.72−3.66 (m, 4H), 2.97−2.80 (m, 2H); MS (ESI): m/z 391.9 (M^+ + H).

*2-(4-Methoxyphenyl)-2-((6-phenylthieno[2,3-d]pyrimidin-4-yl)amino)ethan-1-ol (**25**).* Following the general procedure for the amination of 4-chloro-6-phenylthieno[2,3-*d*]-pyrimidine, compound **25** was obtained as a white solid. ^{1}H NMR (DMSO, 400 MHz): δ 8.28 (s, 1H), 8.21 (s, 1H), 8.01 (d, J = 8.08 Hz, 1H), 7.75−7.67 (m, 2H), 7.55−7.47 (m, 2H), 7.44−7.33 (m, 3H), 6.95−6.84 (m, 2H), 5.48−5.33 (m, 1H), 4.89 (t, J = 5.69 Hz, 1H), 3.91−3.63 (m, 5H); MS (ESI): m/z 378.1 (M^+ + H).

*(R)-2-(4-Methoxyphenyl)-2-((6-phenylthieno[2,3-d]-pyrimidin-4-yl)amino)ethan-1-ol (**26**).* Following the general procedure for the amination of 4-chloro-6-phenylthieno[2,3-*d*]pyrimidine, compound **26** was obtained as a white solid. ^{1}H NMR (DMSO, 400 MHz): δ 8.28 (s, 1H), 8.24 (s, 1H), 8.13 (d, J = 8.2 Hz, 1H), 7.73−7.70 (m, 2H), 7.54−7.50 (m, J = 8.12 Hz, 2H), 7.43−7.39 (m, 1H), 7.37−7.34 (m, 2H), 6.89 (d, J = 8.6 Hz, 2H), 5.43−5.38 (m, 1H), 4.99 (t, J = 6.16 Hz, 1H), 3.79−3.69 (m, 5H); MS (ESI): m/z 378.1 (M^+ + H).

*(S)-2-(4-Methoxyphenyl)-2-((6-phenylthieno[2,3-d]-pyrimidin-4-yl)amino)ethan-1-ol (**27**).* Following the general procedure for the amination of 4-chloro-6-phenylthieno[2,3-

https://dx.doi.org/10.1021/acsinfecdis.0c00300
ACS Infect. Dis. 2021, 7, 1044−1058

d]pyrimidine, compound **27** was obtained as a white solid. ^{1}H NMR (DMSO, 400 MHz): δ 8.28 (s, 1H), 8.24 (s, 1H), 8.14 (d, J = 7.76 Hz, 1H), 7.72 (d, J = 8.2 Hz, 2H), 7.52 (t, J = 7.72 Hz, 2H), 7.43−7.35 (m, 3H), 6.89 (d, J = 9 Hz, 2H), 5.41 (q, J = 7.88 Hz, 1H), 4.99 (t, J = 6.04 Hz, 1H), 3.79−3.69 (m, 5H); MS (ESI): m/z 378.1 (M^+ + H).

*(R)-2-Phenyl-2-((6-phenylthieno[2,3-d]pyrimidin-4-yl)-amino)ethan-1-ol (**28**).* Following the general procedure for the amination of 4-chloro-6-phenylthieno[2,3-*d*]pyrimidine, compound **28** was obtained as a white solid. ^{1}H NMR ($CDCl_3$, 400 MHz): δ 8.46 (s, 1H), 7.69 (d, J = 6.88 Hz, 2H), 7.47−7.34 (m, 9H), 5.85 (s, 1H), 5.50−5.47 (m, 1H), 4.17−4.09 (m, 2H); MS (ESI): m/z 348.9 (M^+ + H).

*(R)-2-(2-Fluoro-4-methoxyphenyl)-2-((6-phenylthieno-[2,3-d]pyrimidin-4-yl)amino)ethan-1-ol (**29**).* Following the general procedure for the amination of 4-chloro-6-phenylthieno[2,3-*d*]pyrimidine, compound **29** was obtained as a yellow solid. ^{1}H NMR ($CDCl_3$, 400 MHz): δ 8.45 (s, 1H), 7.67 (d, J = 6.16 Hz, 2H), 7.45−7.29 (m, 5H), 6.70 (s, 2H), 6.02 (s, 1H), 5.70 (s, 1H), 4.14−4.05 (m, 2H), 3.81 (s, 3H); MS (ESI): m/z 396.01 (M^+ + H).

*(R)-2-(3-Fluoro-4-methoxyphenyl)-2-((6-phenylthieno-[2,3-d]pyrimidin-4-yl)amino)ethan-1-ol (**30**).* Following the general procedure for the amination of 4-chloro-6-phenylthieno[2,3-*d*]pyrimidine, compound **30** was obtained as a yellow solid. ^{1}H NMR ($CDCl_3$, 400 MHz): δ 8.42 (s, 1H), 7.67−7.65 (m, 2H), 7.54 (s, 1H), 7.45−7.35 (m, 3H), 7.22−7.16 (m, 2H), 6.98 (t, J = 8.6 Hz, 1H), 6.31 (s, 1H), 5.45−5.41 (m, 1H), 4.14−4.06 (m, 2H), 3.90 (s, 3H); MS (ESI): m/z 397.3 (M^+ + H).

*(R)-2-((5,6-Dimethylthieno[2,3-d]pyrimidin-4-yl)amino)-2-phenylethan-1-ol (**37**).* Following the general procedure for the amination of 4-chloro-6-phenylthieno[2,3-*d*]pyrimidine, compound **37** was obtained as a white solid. ^{1}H NMR ($CDCl_3$, 400 MHz): δ 8.35(s, 1H), 7.44−7.28 (m, 5H), 6.28 (s, 1H), 5.47−5.43 (m, 1H), 4.07 (d, J = 4.58 Hz, 2H), 2.51 (s, 3H), 2.46 (s, 3H); MS (ESI): m/z 301.00 (M^+ + H).

*(R)-2-((5-Methyl-6-phenylthieno[2,3-d]pyrimidin-4-yl)-amino)-2-phenylethan-1-ol (**38**).* Following the general procedure for the amination of 4-chloro-6-phenylthieno[2,3-*d*]pyrimidine, compound **38** was obtained as a white solid. ^{1}H NMR ($CDCl_3$, 400 MHz): δ 8.48 (s, 1H), 7.48−7.36 (m, 9H), 7.11−7.07 (m, 1H), 5.89 (d, J = 6.84 Hz, 1H), 5.49 (q, J = 5.44 Hz, 1H), 4.17−4.09 (m, 2H), 1.28 (s, 3H); MS (ESI): m/z 361.9 (M^+ + H).

*(R)-2-((6-Methyl-5-phenylthieno[2,3-d]pyrimidin-4-yl)-amino)-2-phenylethan-1-ol (**39**).* Following the general procedure for the amination of 4-chloro-6-phenylthieno[2,3-*d*]pyrimidine, compound **39** was obtained as a white solid. ^{1}H NMR ($CDCl_3$, 400 MHz): δ 8.42 (s, 1H), 7.57 (t, J = 7.63 Hz, 1H), 7.45−7.41 (m, 2H), 7.27−7.21 (m, 5H), 6.90−6.88 (m, 2H), 5.33 (d, J = 5.6 Hz, 1H), 5.20−5.16 (m, 1H), 3.78−3.69 (m, 2H), 2.33 (s, 3H); MS (ESI): m/z 361.9 (M^+ + H).

*(R)-2-Phenyl-2-((5-phenylthieno[2,3-d]pyrimidin-4-yl)-amino)ethan-1-ol (**40**).* Following the general procedure for the amination of 4-chloro-6-phenylthieno[2,3-*d*]pyrimidine, compound **40** was obtained as a white solid. ^{1}H NMR ($CDCl_3$, 400 MHz): δ 8.45 (s, 1H), 7.69−7.67 (m, 2H), 7.47−7.35 (m, 9H), 5.96−5.94 (m, 1H), 5.51−5.47 (m, 1H), 4.17−4.10 (m, 2H); MS (ESI): m/z 348.1 (M^+ + H).

*tert-Butyl (R)-(1-(3-Fluoro-4-methoxyphenyl)-2-hydroxyethyl)carbamate (**33**).* Di-*tert*-butyl dicarbonate (0.290 g, 1.329 mmol) was added to a solution of (*R*)-1-(3-fluoro-4-methoxyphenyl)-2-hydroxyethanaminium chloride **32** (0.267 g, 1.208 mmol) and triethylamine (0.506 mL, 3.63 mmol) in dichloromethane (4 mL). The reaction mixture was stirred for 2 h at room temperature. The mixture was concentrated and purified by flash column chromatography (Isolera 1, Biotage, 10 g size, elution gradient of 12−80% ethyl acetate in hexanes). Pure fractions were evaporated to afford **33** as a white solid. ^{1}H NMR ($CDCl_3$, 500 MHz): δ 7.08−7.03 (m, 2H), 6.96 (t, J = 8.33 Hz, 1H), 5.21 (d, J = 6.55 Hz, 1H), 4.73 (s, 1H), 3.90−3.81 (m, 5H), 2.11 (s, 1H), 1.46 (s, 9H); MS (ESI): m/z 284.3 (M^+ + H).

*tert-Butyl (R)-(2-(1,3-Dioxoisoindolin-2-yl)-1-(3-fluoro-4-methoxyphenyl)ethyl)carbamate (**34**).* Diisopropyl azodicarboxylate (0.282 mL, 1.458 mmol) was added dropwise at room temperature to a solution of **33** (0.320 g, 1.122 mmol), phthalimide (0.215 g, 1.458 mmol), and Ph_3P (0.382 g, 1.458 mmol) in THF (3.8 mL). The resulting mixture was stirred for 16 h at room temperature. The mixture was extracted with ethyl acetate/water, and the organic phase was washed with brine, dried (Na_2SO_4), and evaporated *in vacuo*. The residue was purified by flash column chromatography (Isolera 1, Biotage, 10 g size, elution gradient of 12−60% ethyl acetate in hexanes) to afford **34** as a yellow solid. ^{1}H NMR ($CDCl_3$, 500 MHz): δ 7.80 (m, 2H), 7.66 (m, 2H), 7.04 (m, 2H), 6.87 (m, 1H), 5.28 (d, J = 8.1 Hz, 1H), 4.94−4.92 (m, 1H), 3.89−3.81 (m, 5H), 1.20 (s, 9H); MS (ESI): m/z 415.7 (M^+ + H).

*(R)-2-(2-Amino-2-(3-fluoro-4-methoxyphenyl)ethyl)-isoindoline-1,3-dione (**35**).* HCl (4 M in 1,4-dioxane, 0.9 mL, 3.6 mmol) was added to a solution of **34** (0.372 g, 0.897 mmol) in a mixture of DCM (2.5 mL) and methanol (1 mL), and the resulting mixture was stirred for 16 h at room temperature. The mixture was subjected to acid−base extraction with ethyl acetate/water, and the organic phase was washed with brine, dried (Na_2SO_4), and concentrated *in vacuo*. The resulting residue **35** (yellow oil) was used in the next step without further purification. ^{1}H NMR (MeOD, 500 MHz): δ 7.88−7.78 (m, 4H), 7.20 (dd, J = 12.4, 2.20 Hz, 1H), 7.08 (dd, J = 8.65, 2.14 Hz, 1H), 7.00(t, J = 8.49 Hz, 1H), 4.25 (t, J = 7.27 Hz, 1H), 3.88−3.84 (m, 5H); MS (ESI): m/z 315.5 (M^+ + H).

*(R)-2-(2-(3-Fluoro-4-methoxyphenyl)-2-((6-phenylthieno-[2,3-d]pyrimidin-4-yl)amino)ethyl)isoindoline-1,3-dione (**36**).* Compound **36** was synthesized following the general procedure for amination of 4-chloro-6-phenylthieno[2,3-*d*]-pyrimidine. ^{1}H NMR ($CDCl_3$, 500 MHz): δ 8.31 (s, 1H), 7.88−7.85 (m, 2H), 7.75−7.73 (m, 4H), 7.54 (s, 1H), 7.49 (t, J = 7.55, 1H), 7.42 (t, J = 7.35 Hz, 1H), 7.25−7.22 (m, 2H), 6.99−6.95 (m, 1H), 6.91 (s, 1H), 5.66−5.62 (m, 1H), 4.24−4.12 (m, 2H), 3.89 (s, 3H); MS (ESI): m/z 525.5 (M^+ + H).

*(R)-1-(3-Fluoro-4-methoxyphenyl)-N^1-(6-phenylthieno-[2,3-d]pyrimidin-4-yl)ethane-1,2-diamine (**31**).* Compound **36** (0.203 g, 0.393 mmol) was dissolved in methanol, and a 80% hydrazine hydrate solution (0.073 mL,1.2 mmol) was added dropwise to the solution at 0 °C. The reaction mixture was stirred for 16 h at room temperature. The mixture was extracted with ethyl acetate/water, and the organic phase was washed with brine, dried (Na_2SO_4), and evaporated *in vacuo*. The residue was purified by flash column chromatography (Isolera 1, Biotage, 10 g size, elution gradient of 2−20% methanol in ethyl acetate) to afford **31** as a yellow solid. ^{1}H NMR (DMSO, 500 MHz): δ 8.27 (s, 1H), 8.15 (s, 1H), 7.75 (d, 2H, J = 7.6 Hz), 7.54 (t, 2H, J = 7.6 Hz), 7.44 (t, 1H, J = 7.6 Hz), 7.26 (dd, J = 12.5, 2 Hz, 1H), 7.20 (d, 1H, J = 7.6

https://dx.doi.org/10.1021/acsinfecdis.0c00300
ACS Infect. Dis. 2021, 7, 1044−1058

Hz), 7.12 (t, J = 8.6 Hz, 1H), 5.28−5.25 (m, 1H), 3.80 (s, 3H), 3.00−2.91 (m, 2H), 1.25−1.18 (m, 2H); MS (ESI): m/z 396.4 (M^+ + H).

***H. pylori* IC_{50} Dose Responses.** *H. pylori* strains ATCC 43504, SS1, or SS1 NuoD A402P were grown overnight in Brucella broth containing Skirrow's selective medium supplement and 10% fetal bovine serum (FBS) or brain heart infusion broth containing Skirrow's and 10% FBS. Cultures were grown in vented 25 cm^2 tissue culture flasks at 37 °C and 10% CO_2 with rotation at 50 rpm. 2-Fold serial dilutions of test and control compounds were performed in DMSO or water as appropriate, and 1 μL was transferred to a 96 well plate. 99 μL of a 1:10 dilution of an overnight culture of *H. pylori* in Brucella/Skirrow's/10% FBS was added to each well. Plates were incubated for 18−20 h, and 5 μL of 3 mM resazurin was added to each well. Plates were incubated for an additional 3−5 h, and resazurin reduction was measured using a BioTek Synergy Mx (BioTek, Winooski, VT) with an excitation wavelength of 540 nm and emission read at 590 nm. Percent inhibition compared to growth controls was calculated, and the 50% inhibitory concentration (IC_{50}) was determined using XLFit software (IDBS, London, United Kingdom). pIC_{50}, the negative log of the IC_{50} value when converted to molar units, was calculated on the basis of the individual IC_{50} values along with the standard error of the mean (SEM). All pIC_{50} data with 4 or more independent replicates were analyzed for outliers using Grubbs's test with α set to 0.05 (GraphPad Prism). A t test was used to compare the replicate pIC_{50} values for SS1 wild-type and NuoD A402P mutant (GraphPad Prism). P-values < 0.05 were considered significant.

Cytotoxicity Assays. FaDu (ATCC HTB-43) and HepG2 (ATCC HB-8065) cell lines were routinely maintained according to the protocols provided by the American Type Culture Collection (ATCC). For cytotoxicity IC_{50} determination, 100 μL of cell suspension in Eagle's Minimal Essential Medium (EMEM) supplemented with 10% FBS was seeded into black sided, tissue culture treated 96 well plates (Corning 3603) at a concentration of 3 × 10^5 cells/mL. Plates were incubated for 24 h in a 37 °C, 5% CO_2 incubator to allow for cell adhesion and growth. Spent media was aspirated from the test plates, and serial 2-fold dilutions of test compounds mixed with fresh EMEM + 10% FBS were added to the plates at 100 μL per well. The plates were incubated for 72 h. The media was aspirated, and FBS-free EMEM and resazurin (final concentration of 0.15 mM) were added to the plate. Plates were incubated for 3−5 h, and, then resazurin reduction was measured using a BioTek Synergy Mx (BioTek, Winooski, VT) with an excitation wavelength of 540 nm and emission read at 590 nm. Percent inhibition compared to growth controls was calculated, and the 50% inhibitory concentration (IC_{50}) curves were generated using XLFit software (IDBS, London, United Kingdom). IC_{50} values were converted to pIC_{50} values as described above and the average and SEM were calculated.

Generation of Resistant Mutants, Sequencing, and Target Identification. Mutants resistant to the thienopyrimidine series were generated in two separate ways. Strain HM-274 was chosen for these studies, since it had been previously sequenced and annotated. Spontaneous mutants of HM-274 were selected by concentrating and harvesting susceptible wild-type cultures and spreading them onto plates containing twice the minimum inhibitory concentration (MIC) of **28**. Two stably resistant isolates were recovered that had MICs 8-fold higher than the wild-type. In the second method, *H. pylori* ATCC 43504 was serially passaged onto plates containing increasingly higher concentrations of **1** until the strain was able to grow at 8× the MIC of the wild-type. The DNA from this resistant mutant was then purified and transformed into strain HM-274 to confirm stable genetically transferable resistance prior to sequencing. Genomic DNA was purified from the three resistant mutants as well as HM-274 wild-type using ZR Fungal/Bacterial DNA MiniPrep (Zymo Research) according to the manufacturer's instructions. Whole genome sequencing was performed by Tufts Medical Center. Genome annotation was accomplished using RAST, and single nucleotide polymorphism (SNP) identification was performed with CLC Workbench. The two spontaneous resistant mutants had SNPs in *nuoD*, which caused one amino acid change, either A402P or T400I. The serial passage mutant had multiple nonsynonymous mutations in *nuoD*. There were no other mutations shared by all three strains and not present in the isogenic background strain.

Seven additional spontaneous resistant mutants were subsequently isolated using the same methodology. Genomic DNA was purified from each, and *nuoD* was amplified by PCR. The PCR products were sequenced and compared to wild-type *nuoD*. All seven had mutations in *nuoD* resulting in an amino acid change, either A402P or T400I.

In order to ensure that no secondary mutations were causing thienopyrimidine resistance, a wild-type copy of *nuoD* was modified to contain the A402P mutation using the Q5 Site Directed Mutagenesis kit (New England Biolabs) according to the manufacturer's instructions. The mutation was confirmed by PCR and sequencing, and then, wild-type SS1 was transformed with this plasmid and selected for on plates containing **28**. The A402P mutation in *nuoD* conferred resistance in strain SS1. Several colonies were chosen, and the mutation was confirmed by PCR and sequencing. An SS1 isolate with the NuoD A402P mutation was used in further testing to confirm on target activity of the thienopyrimidine series (see above).

***Ex Vivo* Efficacy Study.** This model was adapted from the standard mouse model of *H. pylori* infection using SS1. Briefly, 6 to 8 week-old female C57BL/6 (specific-pathogen-free) mice were obtained from Charles River Laboratories. Five mice were housed per cage and allowed to acclimate for at least 72 h. Animals were inoculated by oral gavage, three times within 1 week with 0.2 mL of an *H. pylori* SS1 suspension (~10^9 CFU/dose). The infection was allowed to stabilize for 1 to 2 weeks after the final gavage. Mice were euthanized, and the stomachs were excised, bisected laterally into equal halves along the long curvature, and washed three times with sterile PBS. Each half was added to the well of a 12 well plate containing Brucella broth supplemented with 10% FBS and Skirrow's with or without 100× the MIC of compound **25**. Each half from individual stomachs was assigned to a control and treatment group. After 24 h, the stomach halves were washed, weighed, homogenized, serially diluted, and plated on selective medium. These plates were incubated for 7 days, and then, colonies were counted to determine the *H. pylori* burden. Data was log transformed, and statistical significance was determined using a Mann−Whitney test with GraphPad Prism software. A P-value less than 0.05 was considered significant. The study was repeated to ensure reproducibility. Animal use complied with the Animal Welfare Act, the Guide for the Care and Use of Laboratory Animals, and the Office of Laboratory Animal Welfare.

https://dx.doi.org/10.1021/acsinfecdis.0c00300
ACS Infect. Dis. 2021, 7, 1044−1058

Computational Studies of *H. pylori*'s Complex I. *General Computational Methods.* The sequence analysis of *T. thermophilus* and *H. pylori* was done using the online Clustal Omega tool. For residue numbering, a multiple sequence alignment was performed with *M. musculus*, *B. taurus*, *H. sapiens*, *A. fumagatis*, *H. pylori*, *E. coli*, and *M. tuberculosis* using CLC Genomic Workbench 11. Schrödinger's Maestro was used to build three comparative models and for docking.[35] AMBERMD was used to run all simulations.[36]

Homology Modeling. A homology model of the subunits NuoD and NuoB of NADH/ubiquinone oxidoreductase in *Helicobacter pylori* was created using Schrödinger's Phase program.[37] The comparative model was created using a *Thermus thermophilus* protein sequence as a template (PDB: 4HEA). An additional homology model was built with a A402P mutation in the NuoD subunit using the same template. Both models were built using energy-based methods. The comparative models were then prepared by AMBERMD's Leap and then minimized using the steepest decent for 10 000 steps using AMBERMD's PMEMD implementation.[36]

Molecular Docking. A series of thienopyrimidines and piericidin A was docked using Schrödinger's Induced Fit docking based upon the quinone binding channel, based on previous *Thermus thermophilus* and mitochondrial studies of ubiquinone binding (Y85, R40, V403, and N401), mutations found from the Mills et al.[20] group (G398, F404, and V407), and a ligand in our thienopyrimidine series (T400 and A402).[14,18,19,23,33] All residue numbers are based on the protein sequence of *H. pylori*. The default protocol was used with a box size that was extended to allow docking of ligands with up 30 Å in length and sampled each ligand conformation using an energy window of 2.5 kcal/mol for ring conformation sampling and an energy penalty for nonplanar amide bond conformations.[38] The ligands were prepared in Schrödinger using LigPrep.[39] The best poses were chosen using the induced-fit docking (IFD) score (a combination of Glide Score and Prime energy calculations) and visual inspection.[38] The glide scores are representative ranking of ligands based upon the specific molecular docking run based on the interactions between ligand and protein. The thienopyrimidines were docked using the same methods into the T400I model and A402P model. The ligands were then compared using the IFD score.

Molecular Simulations. AMBERMD was used for molecular dynamic simulations. The chosen poses from the molecular docking were parametrized using Leap.[36] The protein−ligand complex was solvated using TIP3P with a 12.0 Å octahedron periodic box and neutralized with Na. The apo protein was subjected to the same solvation and neutralization methods as the protein−ligand complex. The parametrized structures were saved, and the protein−ligand complex was used for simulations using GPU accelerated PMEMD.[36] The ligand−protein complex was minimized using the steepest decent for 10 000 steps utilizing the SHAKE algorithm. The minimized protein−ligand complex was then heated using 2 fs time steps over 50 000 steps to reach 303 K. The heated structure was equilibrated for 20 ns and then further subjected to a 250 ns production run using 2 fs time steps. After the simulation was completed, the AMBER MM-PBSA protocol was used to calculate binding energies and ptraj was used for analysis of protein−ligand interactions.[36] All images were created using UCSF Chimera.[40]

■ ASSOCIATED CONTENT

Supporting Information

The Supporting Information is available free of charge at https://pubs.acs.org/doi/10.1021/acsinfecdis.0c00300.

Table S1: *in vitro* ADME profile of compound **25**; Table S2: mouse pharmacokinetic profile of compound **25**; Table S3: MIC values of select thienopyrimidines against a panel of representative Gram-negative and Gram-positive species; Figure S1: a comparison of pIC_{50} values between SS1 and SS1 A402P mutant; Figure S2: multiple species sequence alignment of respiratory complex I thienopyrimidine binding site; Figure S3: docked conformations of known complex I ligands and inhibitors; Figure S4: a complete energy profile of the protein ligand complex; Figure S5: *in vivo* efficacy of compound **25**; Figure S6: structures of the optimized benzimidazole and omeprazole (PDF)

■ AUTHOR INFORMATION

Corresponding Author

Richard E. Lee − *Department of Chemical Biology and Therapeutics, St. Jude Children's Research Hospital, Memphis, Tennessee 38105, United States;* orcid.org/0000-0002-2397-0443; Email: Richard.Lee@stjude.org

Authors

Alex K. Mugengana − *Department of Chemical Biology and Therapeutics, St. Jude Children's Research Hospital, Memphis, Tennessee 38105, United States; Department of Pharmaceutical Sciences, University of Tennessee Health Science Center, Memphis, Tennessee 38163, United States*

Nicole A. Vita − *Department of Chemical Biology and Therapeutics, St. Jude Children's Research Hospital, Memphis, Tennessee 38105, United States; Department of Pharmaceutical Sciences, University of Tennessee Health Science Center, Memphis, Tennessee 38163, United States*

Autumn Brown Gandt − *Arietis Pharma, Boston, Massachusetts 02118, United States*

Kevin Moran − *Arietis Pharma, Boston, Massachusetts 02118, United States*

George Agyapong − *Arietis Pharma, Boston, Massachusetts 02118, United States*

Lalit K. Sharma − *Department of Chemical Biology and Therapeutics, St. Jude Children's Research Hospital, Memphis, Tennessee 38105, United States*

Elizabeth C. Griffith − *Department of Chemical Biology and Therapeutics, St. Jude Children's Research Hospital, Memphis, Tennessee 38105, United States*

Jiuyu Liu − *Department of Chemical Biology and Therapeutics, St. Jude Children's Research Hospital, Memphis, Tennessee 38105, United States*

Lei Yang − *Department of Chemical Biology and Therapeutics, St. Jude Children's Research Hospital, Memphis, Tennessee 38105, United States*

Ekaterina Gavrish − *Arietis Pharma, Boston, Massachusetts 02118, United States*

Kirk E. Hevener − *Department of Pharmaceutical Sciences, University of Tennessee Health Science Center, Memphis, Tennessee 38163, United States;* orcid.org/0000-0002-5584-3625

Michael D. LaFleur − *Arietis Pharma, Boston, Massachusetts 02118, United States*

https://dx.doi.org/10.1021/acsinfecdis.0c00300
ACS Infect. Dis. 2021, 7, 1044−1058

Complete contact information is available at:
https://pubs.acs.org/10.1021/acsinfecdis.0c00300

Author Contributions

[▽]A.K.M., N.A.V., and A.B.G. contributed equally to this study.

Notes

The authors declare no competing financial interest.

■ ACKNOWLEDGMENTS

The research reported in this publication was supported by the National Institute of Allergy and Infectious Diseases of the National Institutes of Health under award number AI102452 and by ALSAC, St. Jude Children's Research Hospital. The content is solely the responsibility of the authors and does not necessarily represent the official views of the National Institute of Health or other funding agencies. We kindly thank Robin Lee for her assistance in editing the manuscript. Molecular graphics and analyses were performed with UCSF Chimera, developed by the Resource for Biocomputing, Visualization, and Informatics at the University of California, San Francisco, with support from NIH P41-GM103311.

■ REFERENCES

(1) Chey, W. D, Leontiadis, G. I, Howden, C. W, and Moss, S. F (2017) ACG Clinical Guideline: Treatment of Helicobacter pylori Infection. *Am. J. Gastroenterol. 112* (2), 212−239.

(2) Li, B.-Z., Threapleton, D. E., Wang, J.-Y., Xu, J.-M., Yuan, J.-Q., Zhang, C., Li, P., Ye, Q.-L., Guo, B., Mao, C., and Ye, D.-Q. (2015) Comparative effectiveness and tolerance of treatments for Helicobacter pylori: systematic review and network meta-analysis. *BMJ. 351*, h4052.

(3) Luther, J., Higgins, P. D R, Schoenfeld, P. S, Moayyedi, P., Vakil, N., and Chey, W. D (2010) Empiric quadruple vs. triple therapy for primary treatment of Helicobacter pylori infection: Systematic review and meta-analysis of efficacy and tolerability. *Am. J. Gastroenterol. 105* (1), 65−73.

(4) Marcus, E. A., Sachs, G., and Scott, D. R. (2016) Eradication of Helicobacter pylori Infection. *Curr. Gastroenterol Rep 18* (7), 33.

(5) Shiota, S., Reddy, R., Alsarraj, A., El-Serag, H. B., and Graham, D. Y. (2015) Antibiotic Resistance of Helicobacter pylori Among Male United States Veterans. *Clin. Gastroenterol. Hepatol. 13* (9), 1616−1624.

(6) Gavrish, E., Shrestha, B., Chen, C., Lister, I., North, E. J., Yang, L., Lee, R. E., Han, A., Williams, B., Charnuska, D., Coleman, K., Lewis, K., and LaFleur, M. D. (2014) In vitro and in vivo activities of HPi1, a selective antimicrobial against Helicobacter pylori. *Antimicrob. Agents Chemother. 58* (6), 3255−3260.

(7) Bugge, S., Kaspersen, S. J., Larsen, S., Nonstad, U., Bjørkøy, G., Sundby, E., and Hoff, B. H. (2014) Structure-activity study leading to identification of a highly active thienopyrimidine based EGFR inhibitor. *Eur. J. Med. Chem. 75*, 354.

(8) Golub, A. G., Bdzhola, V. G., Briukhovetska, N. V., Balanda, A. O., Kukharenko, O. P., Kotey, I. M., Ostrynska, O. V., and Yarmoluk, S. M. (2011) Synthesis and biological evaluation of substituted (thieno[2,3-d]pyrimidin-4-ylthio)carboxylic acids as inhibitors of human protein kinase CK2. *Eur. J. Med. Chem. 46* (3), 870−876.

(9) Ishikawa, F., Kosasayama, A., Yamaguchi, H., Watanabe, Y., Saegusa, J., Shibamura, S., Sakuma, K., Ashida, S., and Abiko, Y. (1981) Cyclic guanidines. 14. Imidazo[1,2-a]thienopyrimidin-2-one derivatives as blood platelet aggregation inhibitors. *J. Med. Chem. 24* (4), 376−382.

(10) Revelant, G., Dunand, S., Hesse, S., and Kirsch, G. (2011) Microwave-assisted synthesis of 5-substituted 2- aminothiophenes starting from arylacetaldehydes. *Synthesis 2011* (18), 2935−2940.

(11) Richter, M. F., Drown, B. S., Riley, A. P., Garcia, A., Shirai, T., Svec, R. L., and Hergenrother, P. J. (2017) Predictive rules for compound accumulation yield a broad-spectrum antibiotic. *Nature 545* (7654), 299−304.

(12) Addie, M., Ballard, P., Buttar, D., Crafter, C., Currie, G., Davies, B. R., Debreczeni, J., Dry, H., Dudley, P., Greenwood, R., Johnson, P. D., Kettle, J. G., Lane, C., Lamont, G., Leach, A., Luke, R. W. A., Morris, J., Ogilvie, D., Page, K., Pass, M., Pearson, S., and Ruston, L. (2013) Discovery of 4-amino-N-[(1S)-1-(4-chlorophenyl)-3-hydroxypropyl]-1-(7H-pyrrolo[2,3-d]pyrimidin −4-yl)piperidine-4-carboxamide (AZD5363), an orally bioavailable, potent inhibitor of Akt kinases. *J. Med. Chem. 56* (5), 2059−2073.

(13) Sen, S. E., and Roach, S. L. (1995) A convenient two-step procedure for the synthesis of substituted allylic amines from allylic alcohols. *Synthesis 1995* (7), 756−758.

(14) Sazanov, L. A. (2007) Respiratory complex I: mechanistic and structural insights provided by the crystal structure of the hydrophilic domain. *Biochemistry 46* (9), 2275−2288.

(15) Smith, M. A., Finel, M., Korolik, V., and Mendz, G. L. (2000) Characteristics of the aerobic respiratory chains of the microaerophiles Campylobacter jejuni and Helicobacter pylori. *Arch. Microbiol. 174* (1−2), 1−10.

(16) Yagi, T., and Matsuno-Yagi, A. (2003) The proton-translocating NADH-quinone oxidoreductase in the respiratory chain: the secret unlocked. *Biochemistry 42* (8), 2266−2274.

(17) Yagi, T., Yano, T., Di Bernardo, S., and Matsuno-Yagi, A. (1998) Procaryotic complex I (NDH-1), an overview. *Biochim. Biophys. Acta, Bioenerg. 1364* (2), 125−133.

(18) Baradaran, R., Berrisford, J. M., Minhas, G. S., and Sazanov, L. A. (2013) Crystal structure of the entire respiratory complex I. *Nature 494* (7438), 443−8.

(19) Brandt, U. (2006) Energy converting NADH:quinone oxidoreductase (complex I). *Annu. Rev. Biochem. 75*, 69−92.

(20) Mills, S. D., Yang, W., and MacCormack, K. (2004) Molecular characterization of benzimidazole resistance in Helicobacter pylori. *Antimicrob. Agents Chemother. 48* (7), 2524−2530.

(21) Carcanague, D., Shue, Y.-K., Wuonola, M. A., Uria-Nickelsen, M., Joubran, C., Abedi, J. K., Jones, J., and Kuhler, T. C. (2002) Novel Structures Derived from 2-[[(2-Pyridyl)Methyl]Thio]-1H-Benzimidazole as Anti-Helicobacter Pylori Agents, Part 2. *J. Med. Chem. 45* (19), 4300−4309.

(22) Parey, K., Haapanen, O., Sharma, V., Köfeler, H., Züllig, T., Prinz, S., Siegmund, K., Wittig, I., Mills, D. J., Vonck, J., Kühlbrandt, W., and Zickermann, V. (2019) High-Resolution Cryo-EM Structures of Respiratory Complex I: Mechanism, Assembly, and Disease. *Sci. Adv. 5* (12), eaax9484.

(23) Uno, S., Kimura, H., Murai, M., and Miyoshi, H. (2019) Exploring the quinone/inhibitor-binding pocket in mitochondrial respiratory complex I by chemical biology approaches. *J. Biol. Chem. 294* (2), 679−696.

(24) Murai, M., and Miyoshi, H. (2016) Current topics on inhibitors of respiratory complex I. *Biochim. Biophys. Acta, Bioenerg. 1857* (7), 884−91.

(25) Zickermann, V., Wirth, C., Nasiri, H., Siegmund, K., Schwalbe, H., Hunte, C., and Brandt, U. (2015) Mechanistic Insight from the Crystal Structure of Mitochondrial Complex I. *Science (Washington, DC, U. S.) 347* (6217), 44−49.

(26) Di, L., Kerns, E. H., Hong, Y., and Chen, H. (2005) Development and application of high throughput plasma stability assay for drug discovery. *Int. J. Pharm. 297* (1-2), 110−119.

(27) Di, L., Kerns, E. H., Li, S. Q., and Petusky, S. L. (2006) High throughput microsomal stability assay for insoluble compounds. *Int. J. Pharm. 317* (1), 54−60.

(28) Richter, M. F., Drown, B. S., Riley, A. P., Garcia, A., Shirai, T., Svec, R. L., and Hergenrother, P. J. (2017) Predictive rules for compound accumulation yield a broad-spectrum antibiotic. *Nature 545* (7654), 299−304.

(29) Marchetti, M., Arico, B., Burroni, D., Figura, N., Rappuoli, R., and Ghiara, P. (1995) Development of a mouse model of Helicobacter pylori infection that mimics human disease. *Science 267* (5204), 1655−1658.

(30) Lee, A, O'Rourke, J, De Ungria, M., Robertson, B, Daskalopoulos, G, and Dixon, M. (1997) A standardized mouse model of Helicobacter pylori infection: introducing the Sydney strain. *Gastroenterology 112* (4), 1386−1397.
(31) George, L. L, Borody, T. J, Andrews, P., Devine, M., Moore-Jones, D., Walton, M., and Brandi, S. (1990) Cure of duodenal ulcer after eradication of Helicobacter pylori. *Med. J. Aust. 153* (3), 145−149.
(32) Bridges, H. R., Jones, A. J. Y., Pollak, M. N., and Hirst, J. (2014) Effects of metformin and other biguanides on oxidative phosphorylation in mitochondria. *Biochem. J. 462* (3), 475−487.
(33) Molina, J. R., Sun, Y., Protopopova, M., Gera, S., Bandi, M., Bristow, C., McAfoos, T., Morlacchi, P., Ackroyd, J., Agip, A. A., Al-Atrash, G., Asara, J., Bardenhagen, J., Carrillo, C. C., Carroll, C., Chang, E., Ciurea, S., Cross, J. B., Czako, B., Deem, A., Daver, N., de Groot, J. F., Dong, J. W., Feng, N., Gao, G., Gay, J., Do, M. G., Greer, J., Giuliani, V., Han, J., Han, L., Henry, V. K., Hirst, J., Huang, S., Jiang, Y., Kang, Z., Khor, T., Konoplev, S., Lin, Y. H., Liu, G., Lodi, A., Lofton, T., Ma, H., Mahendra, M., Matre, P., Mullinax, R., Peoples, M., Petrocchi, A., Rodriguez-Canale, J., Serreli, R., Shi, T., Smith, M., Tabe, Y., Theroff, J., Tiziani, S., Xu, Q., Zhang, Q., Muller, F., DePinho, R. A., Toniatti, C., Draetta, G. F., Heffernan, T. P., Konopleva, M., Jones, P., Di Francesco, M. E., and Marszalek, J. R. (2018) An inhibitor of oxidative phosphorylation exploits cancer vulnerability. *Nat. Med. 24* (7), 1036−1046.
(34) Sjöström, J. E., Kühler, T., and Larsson, H. (1997) Basis for the Selective Antibacterial Activity in Vitro of Proton Pump Inhibitors against Helicobacter Spp. *Antimicrob. Agents Chemother. 41* (8), 1797−1801.
(35) Schrödinger (2019) *Maestro*, Schrodinger, LLC, New York, NY.
(36) Case, D. A., Ben-Shalom, I. Y., Brozell, S. R., Cerutti, D. S., Cheatham, T. E., III, Cruzeiro, V. W. D., Darden, T. A., Duke, R. E., Ghoreishi, D., Gilson, M. K., Gohlke, H., Goetz, A. W., Greene, D., Harris, R., Homeyer, N., Izadi, S., Kovalenko, A., Kurtzman, T., Lee, T. S., LeGra, S., York, D. M., and Kollman, P. A. (2018) *AMBER 2018*, University of California, San Francisco.
(37) Schrödinger (2019) *Phase*, Schrodinger, LLC, New York, NY.
(38) Schrödinger (2019) *Induced Fit Docking Protocol*, Schrödinger, LLC, New York, NY.
(39) Schrödinger (2019) *LigPrep*, Release 2019-4, Schrodinger, LLC, New York, NY.
(40) Pettersen, E. F., Goddard, T. D., Huang, C. C., Couch, G. S., Greenblatt, D. M., Meng, E. C., and Ferrin, T. E. (2004) UCSF Chimera–a visualization system for exploratory research and analysis. *J. Comput. Chem. 25* (13), 1605−12.

https://dx.doi.org/10.1021/acsinfecdis.0c00300
ACS Infect. Dis. 2021, 7, 1044−1058